Photonic bands of metallic systems. II. Features of surface plasmon polaritons

Takunori Ito and Kazuaki Sakoda*
Research Institute for Electronic Science, Hokkaido University, North 12 West 6, Kita-ku, Sapporo 060-0812, Japan
(Received 4 February 2001; published 9 July 2001)

The photonic band structure of a two-dimensional square lattice composed of metallic cylinders was calculated for the *H* polarization by means of the numerical simulation of dipole radiation based on the finite-difference time-domain method. The presence of radiational eigenmodes that originate from surface plasmon polaritons was clearly shown by the symmetry and the localized nature of the field distribution.

DOI: 10.1103/PhysRevB.64.045117 PACS number(s): 78.66.Bz, 41.20.Jb, 02.60.Cb

I. INTRODUCTION

In the preceding paper,[1] which we will refer to as Paper I hereafter, we have demonstrated that the numerical simulation of dipole radiation based on the finite-difference time-domain (FDTD) method[2] gives accurate dispersion curves, lifetimes, and field distributions of the radiational eigenmodes of photonic crystals even when their dielectric constants depend on frequency. As an example, we applied the method to two-dimensional metallic systems characterized by the frequency-dependent dielectric constant of the Drude type in the case of the *E* polarization. The spatial symmetry of the eigenmodes was consistent with the group-theoretical prediction that was obtained by the reduction procedure starting from the plane-wave representation of unperturbed wave functions. This fact implies that the eigenmodes for the *E* polarization are essentially modified plane waves.

In this paper (Paper II), we deal with the *H* polarization for the same system, for which a qualitatively different feature appears. That is the excitation of surface plasmons. The same problem was tried to solve previously by the plane-wave expansion method.[3] However, the convergence of the plane-wave expansion method was bad and it did not give accurate results. The failure essentially came from the localized nature of the eigenmodes of the plasmon polaritons, which was difficult to reproduce by a superposition of a small number of plane waves. The difficulty that generally lies in the treatment of the frequency-dependent dielectric constants by the plane-wave expansion method[1] was another reason. As will be shown in what follows, this problem can be solved by the numerical simulation of dipole radiation based on the FDTD method.

Since the electromagnetic field of the surface plasmons is considerably localized in the vicinity of the metallic cylinders, the radiational eigenmodes of the metallic system that originate from the surface plasmons can be well represented by the plasmon excitation on a single cylinder. We used this feature to classify the symmetry of plasmon polaritons by the group theory. We found that the field distribution obtained by the numerical calculation coincided with this classification. We also found that the dispersion of the surface plasmon polaritons was extremely flat due to their localized nature. This feature may be used to enhance various optical phenomena.[4]

In Sec. II, the resonant states due to the excitation of surface plasmons on a single metallic cylinder will be examined. The symmetry of the surface plasmon polaritons expected by the group theory will be presented in Sec. III. The numerical method and the long-wavelength approximation (LWA) of the dispersion curve will be described in Sec. IV. The numerical results will be presented and compared with the analytical estimation and the prediction by the group theory in Sec. V. In Sec. VI, a brief summary will be given.

II. PLASMON RESONANCE

As we did in Paper I, we assume a two-dimensional square array of metallic cylinders. We denote the lattice constant and the radius of the cylinders by a and r_m, respectively. We also assume a dielectric constant of the Drude type for the metallic region. In this section, we omit its imaginary part for simplicity,

$$\varepsilon_m = \varepsilon_\infty \left(1 - \frac{\omega_p^2}{\omega^2} \right), \tag{1}$$

where ε_∞ and ω_p stand for the dielectric constant at sufficiently high frequencies and the plasma frequency, respectively.

As will be shown in the following sections, the electromagnetic field of the eigenmodes of surface plasmon polaritons are considerably localized around the surface of the metallic cylinders and the overlapping of the field between adjacent cylinders is small. This situation resembles the electronic bands composed of well localized atomic orbitals. For the latter case, the tight-binding approximation based on the linear combination of atomic orbitals (LCAO) describes the actual bands well. We thus examined the *atomic orbitals* for the present problem, that is, the electromagnetic resonant states that originate from the excitation of surface plasmons on a single metallic cylinder that appear for $\omega < \omega_p$.

For this purpose, we assumed a plane wave incident on a single cylinder with the magnetic field parallel to the cylinder (z) axis, and studied the amplitude of the scattered wave. First we express the magnetic field of the incident plane wave with partial waves using polar coordinates, (r, θ). We take the direction of $\theta = 0$ as the direction of the wave vector $\mathbf{k}$ of the incident plane wave. We thus have

$$H_0 e^{i(\mathbf{k}\cdot\mathbf{r}-\omega t)} = H_0 e^{i(kr\cos\theta-\omega t)} = H_0 e^{-i\omega t}\sum_{l=-\infty}^{\infty} J_l(kr)\exp\left\{il\left(\theta+\frac{\pi}{2}\right)\right\} = H_0 e^{-i\omega t}\left[J_0(kr)+2\sum_{l=1}^{\infty} i^l J_l(kr)\cos l\theta\right], \tag{2}$$

where H_0 is the amplitude of the incident wave, $k=|\mathbf{k}|$, and J_l is the Bessel function of the lth order. The wave equation in the polar coordinate system that describes the magnetic field H_z is given by

$$\frac{1}{\varepsilon}\left(\frac{\partial^2}{\partial r^2}+\frac{1}{r}\frac{\partial}{\partial r}+\frac{1}{r^2}\frac{\partial^2}{\partial\theta^2}\right)H_z=-\frac{\omega^2}{c^2}H_z, \tag{3}$$

where ε stands for the position-dependent dielectric constant and c denotes the light velocity in free space.

As usual, we express H_z by the product of two functions $R(r)$ and $\Theta(\theta)$. We then obtain a couple of equations that R and Θ obey,

$$\frac{\partial^2\Theta}{\partial\theta^2}=-\varepsilon\lambda\Theta, \tag{4}$$

$$\left(\frac{\partial^2}{\partial r^2}+\frac{1}{r}\frac{\partial}{\partial r}+\frac{\varepsilon\omega^2}{c^2}-\frac{\varepsilon\lambda}{r^2}\right)R=0, \tag{5}$$

where λ is the parameter for decoupling. Because $\Theta(\theta)$ should be a single-valued function, $\sqrt{\varepsilon\lambda}$ is an integer, which we denote by n. The solutions of Eq. (4) are thus given by

$$\Theta(\theta)\propto e^{in\theta},\quad e^{-in\theta}. \tag{6}$$

For $r>r_m$, we define a new variable s by

$$s=kr. \tag{7}$$

Then Eq. (5) is modified to

$$\left(\frac{\partial^2}{\partial s^2}+\frac{1}{s}\frac{\partial}{\partial s}+1-\frac{n^2}{s^2}\right)R=0. \tag{8}$$

This is the Bessel equation and its solution is given by the Bessel and Neumann functions, both of which are analytic for $r>r_m$:

$$R(r)\propto J_n(kr),\quad N_n(kr). \tag{9}$$

On the other hand, for $r<r_m$, the dielectric constant $\varepsilon_m(\omega)$ is negative for $\omega<\omega_p$. In this case, we have to take

$$s=\kappa r, \tag{10}$$

where

$$\kappa=\sqrt{-\varepsilon_m(\omega)}\frac{\omega}{c}. \tag{11}$$

We thus obtain for $r<r_m$

$$\left[\frac{\partial^2}{\partial s^2}+\frac{1}{s}\frac{\partial}{\partial s}-\left(1+\frac{n^2}{s^2}\right)\right]R=0. \tag{12}$$

This is the modified Bessel equation and its solution is given by the modified Bessel function of the first kind,

$$R(r)\propto I_n(\kappa r), \tag{13}$$

since the modified Bessel function of the second kind is not analytic at $r=0$. When we take into account that the geometry is symmetric with respect to θ, the total field is given by

$$H_z=\sum_{n=0}^{\infty} A_n I_n(\kappa r)\cos n\theta \quad (r<r_m), \tag{14}$$

$$H_z=\sum_{n=0}^{\infty}\left[B_n J_n(kr)+C_n N_n(kr)\right]\cos n\theta \quad (r>r_m), \tag{15}$$

where A_n, B_n, and C_n are constants that should be determined by the boundary conditions.

The independent boundary conditions at $r=r_m$ are the continuity of H_z and $\varepsilon^{-1}\partial H_z/\partial r$. The latter is equivalent to the continuity of the tangential component of the electric field. From these conditions, we obtain

$$\frac{A_n}{B_n}=\frac{k\varepsilon_m[N_n'(kR)J_n(kR)-N_n(kR)J_n'(kR)]}{k\varepsilon_m N_n'(kR)I_n(\kappa R)-\kappa\varepsilon_b N_n(kR)I_n'(\kappa R)}, \tag{16}$$

$$\frac{C_n}{B_n}=-\frac{k\varepsilon_m J_n'(kR)I_n(\kappa R)-\kappa\varepsilon_b J_n(kR)I_n'(\kappa R)}{k\varepsilon_m N_n'(kR)I_n(\kappa R)-\kappa\varepsilon_b N_n(kR)I_n'(\kappa R)}, \tag{17}$$

where ε_b denotes the dielectric constant in the background region. Finally, by comparing Eq. (2) and Eq. (15), we obtain

$$B_0=H_0 \quad\text{and}\quad B_n=2i^n H_0. \tag{18}$$

When we calculated A_n/B_n and C_n/B_n as functions of ω, we observed sharp resonances, which imply the excitation of surface plasmons by the incident plane wave. As an example, Fig. 1 shows the ω dependence of A_n/B_n for $n=1$–5 in which a sharp resonance peak is observed for each curve. No resonance peak was observed with $n=0$. The resonance frequencies are listed in Table I. The resonance frequency converges to $\omega_p/\sqrt{1+\varepsilon_b}$ with increasing n irrespective of the

TABLE I. Comparison between the resonance frequencies in the spectra of A_n/B_n and the eigenfrequencies on the Γ point in the unit of $2\pi c/a$. The same parameters as Fig. 1 were used for the numerical calculation.

n	Resonance frequency	Eigenfrequency
1	0.8194	0.7183
2	0.6149	0.5963,0.6712
3	0.6627	0.6431
4	0.6849	0.6876,0.7037
5	0.6937	-

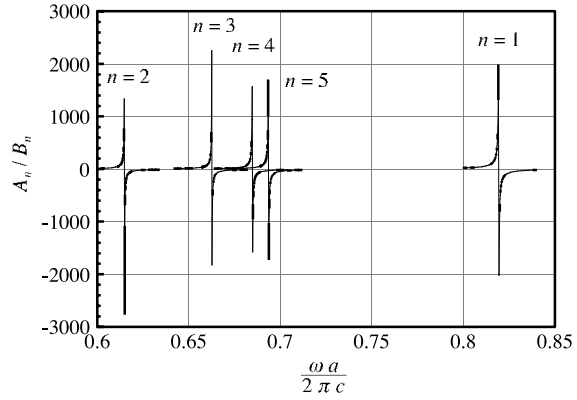

FIG. 1. ω dependence of A_n/B_n for small n. The following parameters were assumed: $\varepsilon_\infty = 1.0$, $\omega_p a/2\pi c = 1.0$, $r_m = 0.3a$, and $\varepsilon_b = 1.0$ (air). A sharp resonance that originates from the excitation of the surface plasmon is observed in each curve.

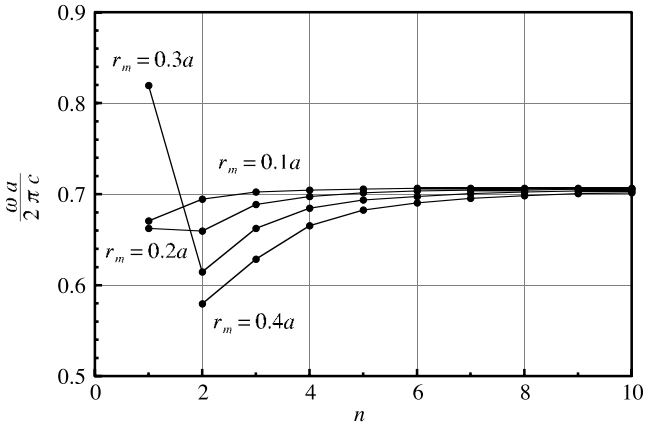

FIG. 2. n dependence of the resonance frequency.

ratio $r_m:a$ as is shown in Fig. 2. This value is the same as that of the surface plasmon on a flat interface between a metal and a dielectric. These resonant states have a finite radiative lifetime and they are not eigenmodes of the system. However, when the metallic cylinders are arrayed in the photonic crystal, the resonant states can be propagated from one cylinder to another to become a Bloch eigenstate and obtain the infinite lifetime. Because the resonant states are localized at each cylinder, they may be regarded as atomic orbitals in the theory of LCAO. This feature can be used to classify and predict the symmetry of the eigenmodes that originate from the surface plasmons.

III. SYMMETRY OF PLASMON POLARITONS

In Paper I, we investigated the photonic bands of the two-dimensional metallic lattice for the E polarization in detail. For that case, each dispersion curve in the photonic crystal had its replica in free space. This feature was demonstrated by the comparison of the symmetry of the eigenmodes between the photonic crystal and free space. As for the H polarization, the situation is different. We have modes that originate from the surface plasmons as well, which do not have their replicas in free space. We can classify the symmetry of those eigenmodes by examining the symmetry of the resonant states found in the last section.

First, let us examine the Δ point in the two-dimensional Brillouin zone, i.e., $\mathbf{k}=(k,0)$ where $0<k<\pi/a$. The k group is given by $C_i=\{\hat{E},\hat{\sigma}_y\}$ where $\hat{E}$ is the identity operation and $\hat{\sigma}_y$ is the mirror reflection about the x axis. The eigenfunction on the Δ point is thus either symmetric or antisymmetric about the x axis. On the other hand, the angular (θ) dependence of the resonant state, whose radial variation is described by $I_n(\kappa r)$ for $r<r_m$ and $J_n(kr)$ and $N_n(kr)$ for $r>r_m$, is given by $e^{\pm in\theta}$ for each $n\geqslant 1$, where we measure θ counterclockwise from the x axis. The symmetric and antisymmetric combinations of these two functions, i.e., $\cos n\theta$ and $\sin n\theta$, possess the appropriate symmetry that the exact eigenfunctions should have. We can thus conclude that the resonant states characterized by index n give one symmetric and one antisymmetric modes for the Δ point.

Next, let us examine the Γ point, which has the symmetry of the C_{4v} point group. The spatial variation of the resonant states is illustrated schematically in Fig. 3. When we compare them with the symmetry of the irreducible representations of C_{4v}, which are shown in Fig. 4, the symmetry of the former is easily assigned. The results are also shown in Fig. 3. Similar assignments can be made for the X point, which has the symmetry of the C_{2v} point group. All the results are summarized in Table II. Symmetry assignments are presented for $n=1$–4 in this table. Those for $n'>4$ can be obtained by a simple relation such that the same irreducible representations appear if

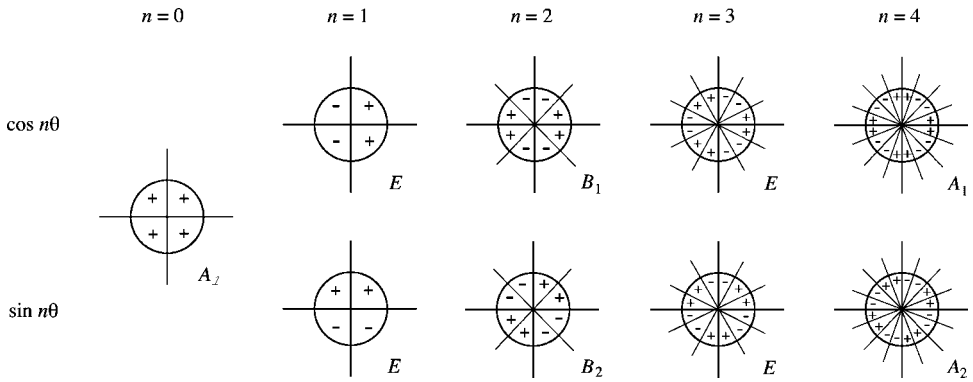

FIG. 3. The angular variation of the magnetic field and the symmetry assignment of the resonant states according to the irreducible representations of the C_{4v} point group.

$$n' = n + 4j, \tag{19}$$

where j is an integer.

IV. PHOTONIC BAND CALCULATION

In Paper I, we derived Maxwell's equations that described the temporal evolution of the electromagnetic field in the presence of metallic components and the oscillating point dipole. When we calculated the dispersion relation of the simple cubic lattice composed of dielectric spheres as a special case, we treated all six components of the field. On the other hand, when we calculated the dispersion relation of the square lattice composed of the metallic cylinders for the E polarization, we only dealt with the z component of the electric field, since the wave equation for E_z was not very singular due to the fact that E_z and its derivatives of the first order are continuous. In the present case, i.e., for the H polarization of the metallic square lattice, H_z is continuous, but its derivatives with respect to the spatial coordinates are generally discontinuous. We thus cannot expect a good convergence when we just deal with H_z.

For the H polarization, the electromagnetic field has three components, that is, H_z, E_x, and E_y, which do not depend on the z coordinate. In this case, the FDTD equation for H_z is given by[5]

$$\begin{aligned} H_z^{p+1/2}(l+\tfrac{1}{2},m+\tfrac{1}{2}) &= H_z^{p-1/2}(l+\tfrac{1}{2},m+\tfrac{1}{2}) \\ &- \frac{\Delta t}{\mu_0}\left[\frac{E_y^p(l+1,m+\tfrac{1}{2})-E_y^p(l,m+\tfrac{1}{2})}{\Delta x} - \frac{E_x^p(l+\tfrac{1}{2},m+1)-E_x^p(l+\tfrac{1}{2},m)}{\Delta y}\right] \\ &+ \frac{i\omega\mu_z\Delta t}{\mu_0\Delta x\Delta y}\,\delta_{ll_0}\delta_{mm_0}e^{-i\omega p\Delta t}, \end{aligned} \tag{20}$$

where μ_0 denotes the magnetic permeability of free space. p, l, and m are integers that specify the discretized t, x, and y coordiates, respectively. For example, $l+1/2$ implies $x=(l+1/2)\Delta x$, $m+1/2$ implies $y=(m+1/2)\Delta y$, and so on. On the other hand, $H_z^{p+1/2}$ implies the z component of the magnetic field at $t=(p+1/2)\Delta t$, and so on. Here, Δt, Δx, and Δy stand for the interval of the representative points in the temporal and spatial meshes. The last term on the right-hand side represents an oscillating magnetic dipole moment located at $((l_0+1/2)\Delta x,(m_0+1/2)\Delta y)$, where its amplitude is denoted by μ_z. We found that the use of a magnetic dipole rather than an electric dipole resulted in somewhat better convergence for the present problem. The FDTD equation for E_x in the metallic cylinder is given by

$$\begin{aligned} E_x^{p+1}(l+\tfrac{1}{2},m) &= E_x^p(l+\tfrac{1}{2},m) + \frac{\Delta t}{\varepsilon_0\varepsilon_\infty\Delta y}\left[H_z^{p+1/2}\left(l+\frac{1}{2},m+\frac{1}{2}\right) - H_z^{p+1/2}(l+\tfrac{1}{2},m-\tfrac{1}{2})\right] \\ &- \omega_p^2(\Delta t)^2\sum_{q=-\infty}^{p} e^{-\gamma(p-q+1/2)}E_x^q\left(l+\frac{1}{2},m\right), \end{aligned} \tag{21}$$

where ε_0 is the permittivity of free space. Here we used the response function given by Eq. (8) of Paper I. On the other hand, the FDTD equation for E_x in the background region with the dielectric constant ε_b is given by

$$\begin{aligned} E_x^{p+1}(l+\tfrac{1}{2},m) &= E_x^p\left(l+\frac{1}{2},m\right) + \frac{\Delta t}{\varepsilon_0\varepsilon_b\Delta y}\left[H_z^{p+1/2}\left(l+\frac{1}{2},m+\frac{1}{2}\right) - H_z^{p+1/2}(l+\tfrac{1}{2},m-\tfrac{1}{2})\right]. \end{aligned} \tag{22}$$

Similar FDTD equations can be obtained easily for E_y.

We solved these equations numerically with initial conditions $\mathbf{E}=\mathbf{0}$ and $\mathbf{H}=\mathbf{0}$, and boundary conditions

$$E_x(\mathbf{r}+\mathbf{a},t) = \exp(i\mathbf{k}\cdot\mathbf{a})E_x(\mathbf{r},t), \tag{23}$$

$$E_y(\mathbf{r}+\mathbf{a},t) = \exp(i\mathbf{k}\cdot\mathbf{a})E_y(\mathbf{r},t), \tag{24}$$

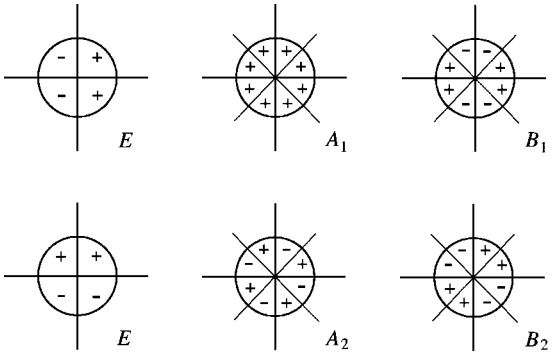

FIG. 4. Symmetry of irreducible representations of the C_{4v} point group.

TABLE II. Symmetry of the eigenmodes expected from the LCAO approximation and the group theory.

n	$\Gamma(C_{4v})$	$\Delta(C_i)$	$X(C_{2v})$
1	E	$A+B$	B_1+B_2
2	B_1+B_2	$A+B$	A_1+A_2
3	E	$A+B$	B_1+B_2
4	A_1+A_2	$A+B$	A_1+A_2

TABLE III. Comparison between the slope of the dispersion curve at the low frequency region obtained by the band calculation (band) and by the long-wavelength approximation (LWA).

r_m/a	ω/ck (band)	ω/ck (LWA)
0.1	0.960	0.984
0.2	0.872	0.935
0.3	0.773	0.847
0.4	0.625	0.705

$$H_z(\mathbf{r}+\mathbf{a},t)=\exp(i\mathbf{k}\cdot\mathbf{a})H_z(\mathbf{r},t), \tag{25}$$

where $\mathbf{k}$ is the wave vector in the two-dimensional first Brillouin zone and $\mathbf{a}$ is the elementary lattice vector. The latter condition extracts the contribution to the radiated electromagnetic field from particular eigenmodes with the specified wave vector. We can thus calculate the dipole radiation spectrum for each $\mathbf{k}$, and its resonance peaks give the eigenfrequencies. The eigenfunctions can be obtained from the field distribution after sufficient cycles of the oscillation of the dipole. Usually, 50 cycles were enough. We calculated the dispersion curves from the Γ point to the X point in the first Brillouin zone assuming the following parameters in Eq. (8) of Paper I: $\varepsilon_b=1.0$ (air), $\varepsilon_\infty=1.0$, $\omega_p a/2\pi c=1.0$, $\gamma=0.01\omega_p$, and $r_m=0.3a$.

Because of the boundary condition, Eqs. (23)–(25), it was enough to deal with only one unit cell, and therefore, the CPU time necessary for the numerical calculation was small. In the actual calculation, the two-dimensional unit cell was divided into 40×40 parts to discretize the Maxwell equations. The further decrease in the size of the spatial and temporal meshes did not bring about an apparent change in the eigenfrequencies.

Let us derive the LWA estimation for the dispersion curve here. We assume that $\gamma=0$, $\omega\ll\omega_p$, and $fc^2k^2\ll\varepsilon_\infty\omega_p^2$, where

$$f=\frac{\pi r_m^2}{a^2} \tag{26}$$

is the filling factor for the metallic cylinders. In this case, the dielectric constant of the Drude type can be approximated by

$$\varepsilon_m(\omega)\approx-\frac{\varepsilon_\infty\omega_p^2}{\omega^2}. \tag{27}$$

The spatial average of the inverse dielectric function is thus given by

$$\overline{\left(\frac{1}{\varepsilon}\right)}\approx-\frac{f\omega^2}{\varepsilon_\infty\omega_p^2}+\frac{1-f}{\varepsilon_b}. \tag{28}$$

The eigenfrequency in the LWA is obtained as

$$\omega\approx\sqrt{\overline{\left(\frac{1}{\varepsilon}\right)}}ck\approx\sqrt{\frac{1-f}{\varepsilon_b}}\left(ck-\frac{fc^3k^3}{2\varepsilon_\infty\omega_p^2}\right). \tag{29}$$

The dispersion curve should thus start from the Γ point and increase approximately linearly with k. The slope of the curve is determined by the filling factor and the dielectric constant of the background region alone and does not depend on other parameters, i.e., ε_∞ or ω_p. The reason is that the electromagnetic field is excluded from the metallic region at sufficiently small frequencies irrespective of ε_∞ and ω_p, and the volume where the field can exist is determined by the filling factor. The slope of the lowest dispersion curve in LWA is listed in Table III for four filling factors that will be examined numerically in the next section.

V. NUMERICAL RESULTS AND DISCUSSION

Figure 5 shows the calculated dispersion relation from the Γ point, $(0,0)$, to the X point, $(\pi/a,0)$, for $r_m=0.3a$ where

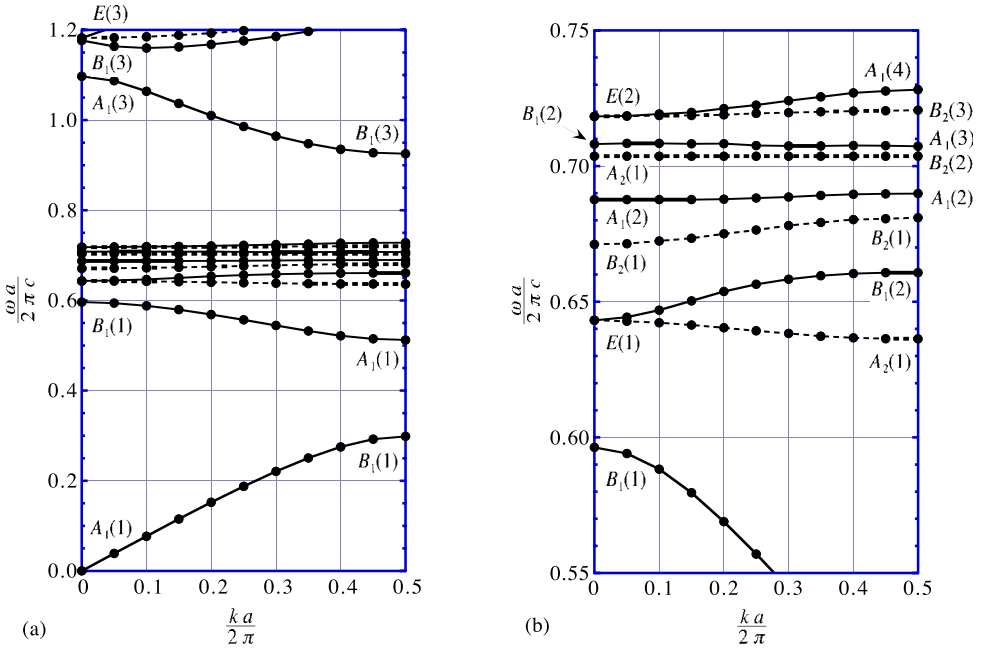

FIG. 5. The dispersion relation from the Γ point to the X point for the radiational eigenmodes in the two-dimensional square lattice composed of metallic cylinders calculated for the H polarization. The following parameters were assumed: $r_m/a=0.3$, $\omega_p a/2\pi c=1.0$, $\gamma=0.01\omega_p$, $\varepsilon_\infty=1.0$, and $\varepsilon_b=1.0$.

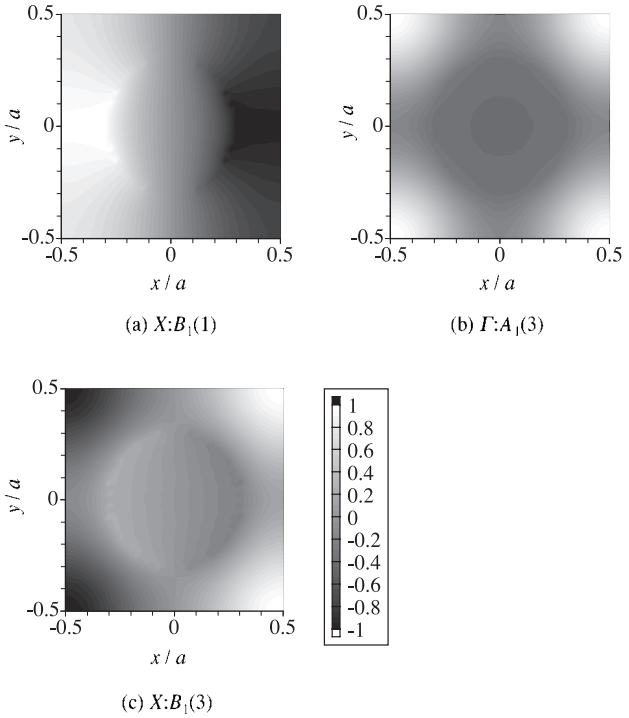

FIG. 6. The distribution of H_z of the (a) $B_1(1)$ mode on the X point, (b) $A_1(3)$ mode on the Γ point, and (c) $B_1(3)$ mode on the X point. The maximum of each magnetic field is normalized to unity.

symmetric (antisymmetric) modes about the x axis are drawn with solid (broken) lines. The symmetries of the eigenmodes on the Γ and X points that were obtained from the calculated field distribution are also shown. The number in parentheses distinguishes the eigenmodes when more than one eigenmode with the same symmetry exists in the analyzed frequency range, $0 \leqslant \omega a/2\pi c \leqslant 1.2$. The spectral region, $\omega a/2\pi c = 0.55$–0.75, is magnified in Fig. 5(b). Those bands with extremely flat dispersion that originate from the surface plasmon polaritons are located in this frequency range. As was predicted by LWA, the lowest dispersion curve starts linearly from $\omega = 0$ at the Γ point. Its slope, which is given in Table III, coincides fairly well with the LWA estimation.

In order to see the nature of the flat bands and confirm the symmetry assignments, let us examine their field distribution. In the following figures, the maximum of the magnetic field is normalized to unity. First, Fig. 6 shows three examples of extended eigenmodes that originate mainly from the radiation field in free space. It is evident that they show their peculiar spatial symmetries. The large bandwidths of the lowest and the seventh lowest symmetric bands reflect the extended nature of their wave functions.

On the other hand, Fig. 7 shows the first example of the localized wave functions of the surface plasmon polaritons. It shows the distribution of H_z of the second lowest E mode, $E(2)$, on the Γ point. Since one mode is the replica of the other given by the 90° rotation, these two modes are degenerate and are attributed to the E representation of the C_{4v} point group. The fields are localized in the vicinity of the surface of the metallic cylinder, and they have the character of the surface plasmon polaritons. Their angular dependence is approximately given by $\cos\theta$ and $\sin\theta$. When we compare these field distributions with those given in Fig. 3, we see that the former originate from the surface plasmon with $n = 1$. Next, let us examine the field distribution of the $B_1(1)$ and $B_2(1)$ modes on the Γ point that are shown in Fig. 8. They are also localized around the cylinder surface and their angular dependence is approximately given by $\cos 2\theta$ and $\sin 2\theta$, which implies that these two modes originate from the surface plasmon polaritons with $n = 2$. Their symmetries are consistent with the group-theoretical prediction presented in Fig. 3 that is based on the LCAO description of the Bloch wave function with single n. However, the symmetries of modes on the X points are inconsistent with this picture. We should thus take into consideration the mixing of the surface plasmons with different n. Actually the $E(2)$ mode on the Γ point connects with the $A_1(4)$ and $B_2(3)$ modes on the X point whose field distributions are presented in Fig. 9. The field distribution of the $B_2(3)$ mode is similar to that of the surface plasmon with $n = 1$, whereas the $A_1(4)$ mode does not correspond to any pattern in Fig. 3. As for the $B_1(1)$ and $B_2(1)$ modes on the Γ point, they connect with the $A_1(1)$ and $B_2(1)$ modes on the X point whose field distributions are shown in Fig. 10. Figure 10(a) somewhat resembles the field pattern of the surface plasmon with $n = 2$, whereas Fig. 10(b) does not. Since the bandwidth of the second lowest symmetric band is fairly large, the mixing with extended modes in the background region may take place.

Among the rest of the eigenmodes found on the Γ point, $E(1)$ and $A_1(2)$,$A_2(1)$ are attributed to the surface plasmon polaritons with $n = 3$ and 4, respectively. Their eigenfrequencies are close to the corresponding resonance frequencies as

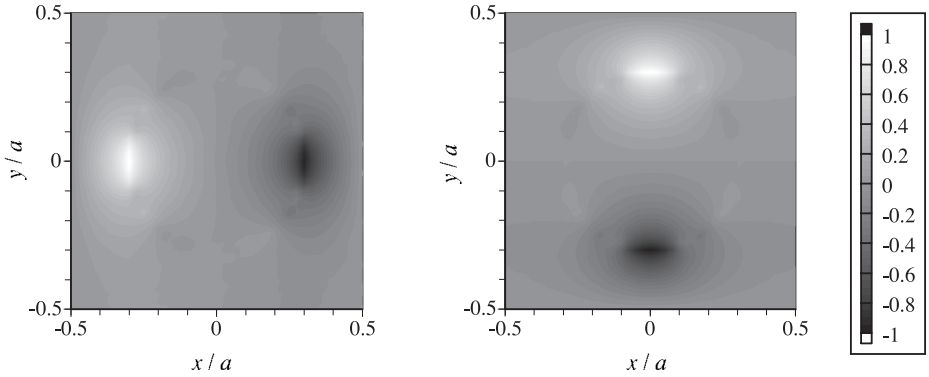

FIG. 7. The distribution of H_z of the $E(2)$ mode on the Γ point. This mode is doubly degenerate and one eigenmode is a replica of the other given by the 90° rotation. The comparison of these distributions with those given in Fig. 3 shows that the $E(2)$ mode has the character of the surface plasmon with $n = 1$.

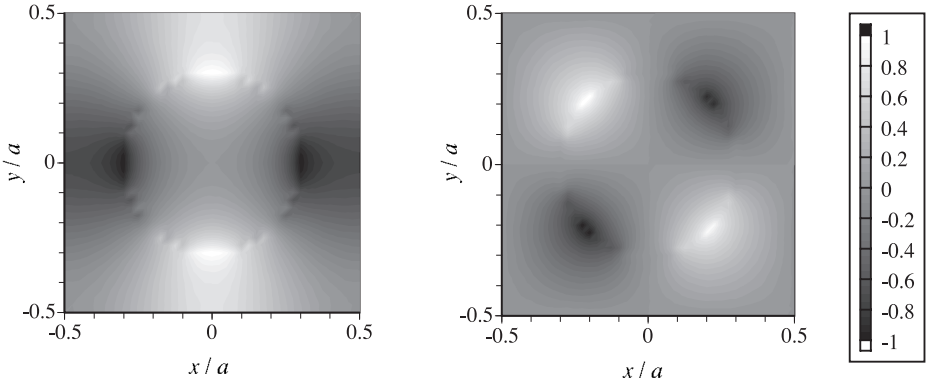

(a) Γ: $B_1(1)$ (b) Γ: $B_2(1)$

FIG. 8. The distribution of H_z of the (a) $B_1(1)$ and (b) $B_2(1)$ modes on the Γ point.

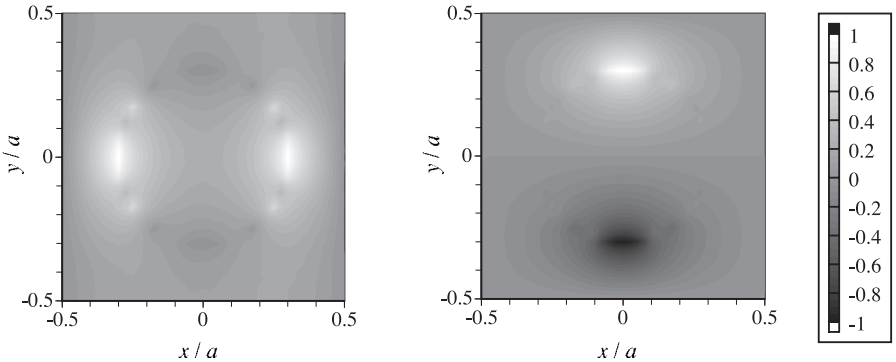

(a) X: $A_1(4)$ (b) X: $B_2(3)$

FIG. 9. The distribution of H_z of the (a) $A_1(4)$ and (b) $B_2(3)$ modes on the X point.

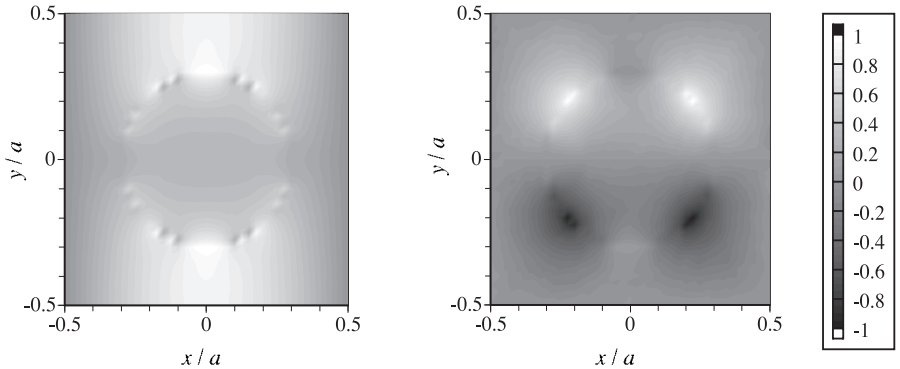

(a) X: $A_1(1)$ (b) X: $B_2(1)$

FIG. 10. The distribution of H_z of the (a) $A_1(1)$ and (b) $B_2(1)$ modes on the X point.

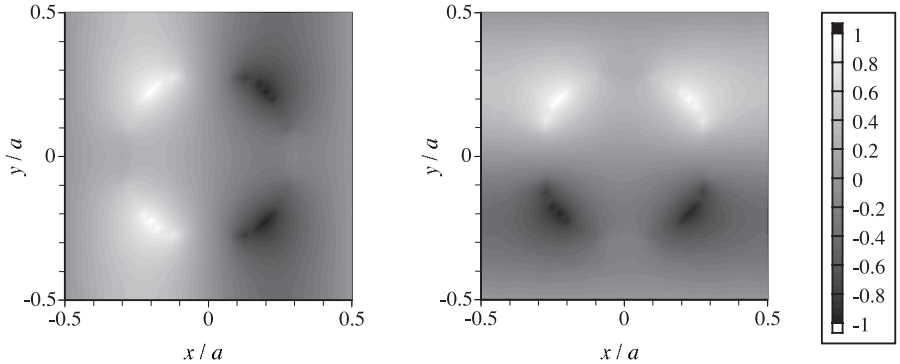

FIG. 11. The distribution of H_z of the $E(1)$ mode on the Γ point.

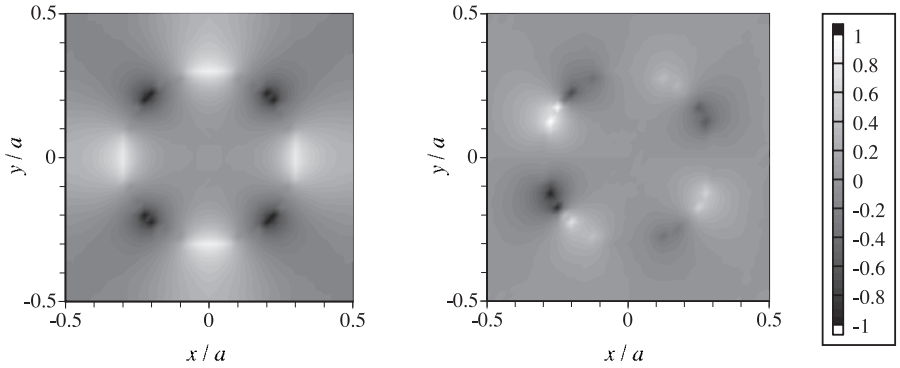

FIG. 12. The distribution of H_z of the (a) $A_1(2)$ and (b) $A_2(1)$ modes on the Γ point.

listed in Table I. Their field distributions are shown in Figs. 11 and 12. The angular dependence of $\cos 4\theta$ and $\sin 4\theta$ can be observed in Fig. 12, whereas the angular dependence in Fig. 11 deviates from that shown in Fig. 3, which implies the mixing of eigenfunctions with other E modes.

In addition to the bands with index $n=1$ to 4 that we reported so far, several unresolved peaks were observed in the dipole radiation spectrum in the vicinity of the converged frequency, $\omega_p/\sqrt{2}$, which may be attributed to surface plasmon polaritons with $n \geqslant 5$. These modes are not shown in Fig. 5. As we examined in Sec. II, an infinite number of plasmon resonance states are expected to exist for the present model with the metallic dielectric constant of the Drude type. Since the wave functions of these higher modes are more localized around the surface of the metallic rod, the LCAO description of the eigenmodes with single n becomes more accurate. We may thus expect that there exist an infinite number of bands with extremely small bandwidths around this frequency. This feature of the two-dimensional metallic system is, of course, brought about by the particular choice of the frequency-dependent dielectric constant. If we adopt a more realistic model by taking into account the interband transition and the spatial dispersion, this infinite degeneracy of the eigenmodes will be removed. As we mentioned in Paper I, the present method for the numerical analysis of the radiaton field in photonic crystals can be extended to frequency-dependent dielectric constants of other types and to the case that the analytical form of the dielectric constant is not known. As for the spatial dispersion of the dielectric constant, we can treat it by carrying out the convolution integral in Eq. (4) of Paper I over **r** as well as t, although the computational task may increase considerably. Thus we can deal with more realistic systems within the scope of the present study.

VI. CONCLUSION

The photonic band structure of the two-dimensional square lattice composed of metallic cylinders characterized by the frequency-dependent dielectric constant of the Drude type was calculated for the H polarization by means of the numerical simulation of dipole radiation based on the FDTD method. The presence of the radiational eigenmodes with extremely small bandwidths that originate from surface plasmons on a single cylinder was clearly seen by the symmetry and the localized nature of the field distribution. We also showed that the LCAO description of the radiational band with a single plasmon resonance state is a fairly accurate approximation for this system.

ACKNOWLEDGMENTS

This work was supported by the Mitsubishi Foundation and the Grant-in-Aid for Scientific Research on Priority Area ''Photonic Crystals'' from the Ministry of Education, Science, Sports, and Culture.

*Electronic address: sakoda@es.hokudai.ac.jp

[1] K. Sakoda, N. Kawai, T. Ito, A. Chutinan, S. Noda, T. Mitsuyu, and K. Hirao, preceding paper, Phys. Rev. B **64**, 045116 (2001).
[2] K. Sakoda and H. Shiroma, Phys. Rev. B **56**, 4830 (1997).
[3] V. Kuzmiak, A.A. Maradudin, and F. Pincemin, Phys. Rev. B **50**, 16 835 (1994).
[4] K. Sakoda and K. Ohtaka, Phys. Rev. B **54**, 5732 (1996).
[5] A. Taflove, *Computational Electrodynamics* (Artech House, Boston, 1995).